Apparent Overinvestment in Leaf Venation Relaxes Leaf Morphological Constraints on Photosynthesis in Arid Habitats[1][OPEN]

Hugo J. de Boer[2]*, Paul L. Drake[2], Erin Wendt, Charles A. Price, Ernst-Detlef Schulze, Neil C. Turner, Dean Nicolle, and Erik J. Veneklaas*

School of Plant Biology (H.J.d.B., P.L.D., E.W., C.A.P., E.J.V.) and Institute of Agriculture (N.C.T., E.J.V.), University of Western Australia, Crawley 6009, Australia; Department of Environmental Sciences, Utrecht University, Utrecht 3584 CS, The Netherlands (H.J.d.B.); Max-Planck Institute for Biogeochemistry, Jena 07745, Germany (E.-D.S.); and Currency Creek Arboretum, Melrose Park 5039, Australia (D.N.)

ORCID ID: 0000-0002-7030-4056 (E.J.V.).

Leaf veins supply the mesophyll with water that evaporates when stomata are open to allow CO_2 uptake for photosynthesis. Theoretical analyses suggest that water is optimally distributed in the mesophyll when the lateral distance between veins (d_x) is equal to the distance from these veins to the epidermis (d_y), expressed as d_x:$d_y \approx 1$. Although this theory is supported by observations of many derived angiosperms, we hypothesize that plants in arid environments may reduce d_x:d_y below unity owing to climate-specific functional adaptations of increased leaf thickness and increased vein density. To test our hypothesis, we assembled leaf hydraulic, morphological, and photosynthetic traits of 68 species from the *Eucalyptus* and *Corymbia* genera (termed eucalypts) along an aridity gradient in southwestern Australia. We inferred the potential gas-exchange advantage of reducing d_x beyond d_y using a model that links leaf morphology and hydraulics to photosynthesis. Our observations reveal that eucalypts in arid environments have thick amphistomatous leaves with high vein densities, resulting in d_x:d_y ratios that range from 1.6 to 0.15 along the aridity gradient. Our model suggests that, as leaves become thicker, the effect of reducing d_x beyond d_y is to offset the reduction in leaf gas exchange that would result from maintaining d_x:d_y at unity. This apparent overinvestment in leaf venation may be explained from the selective pressure of aridity, under which traits associated with long leaf life span, high hydraulic and thermal capacitances, and high potential rates of leaf water transport confer a competitive advantage.

A fundamental challenge for terrestrial plants is to balance the benefit of carbon uptake versus the risk of desiccation resulting from concurrent transpirational water loss. To achieve this, water transport processes in leaves are integrated such that leaf hydraulic properties determine the supply of water to the mesophyll and transpirational losses are regulated by stomatal conductance (g_s; Sack and Scoffoni, 2013). Water enters the leaf as a liquid and is distributed along the plane of the leaf through the xylem in veins. After water exits the vein, it moves through the mesophyll toward the epidermis, where it reaches the stomatal pore as water vapor. Little is known about how exactly water moves from the veins to the stomatal pores and where the liquid-to-gas phase transition occurs (Sack and Holbrook, 2006; Sack and Scoffoni, 2013), yet the length of the postvenous path (l_{H2O}) shows a strong negative relationship with leaf hydraulic conductance (k_{leaf}; Brodribb et al., 2007; Buckley et al., 2015). As a result, several leaf morphological traits, such as leaf vein density, the depth of the veins inside the leaf, and leaf thickness (T_L), influence leaf water transport (Noblin et al., 2008; Buckley et al., 2015). The close relationship between leaf water status and g_s implies that the hydraulic architecture of the leaf poses an important constraint on carbon uptake, specifically in environments with a high evaporative demand.

[1] This work was supported by the Centre of Excellence for Climate Change, Woodland, and Forest Health (State Government of Western Australia), the Australian Research Council (grant no. LP14100736), the Max-Planck Institute, the Netherlands Organization for Scientific Research, and an Endeavour Fellowship.

[2] These authors contributed equally to the article.

* Address correspondence to h.j.deboer@uu.nl or erik.veneklaas@uwa.edu.au.

The author responsible for distribution of materials integral to the findings presented in this article in accordance with the policy described in the Instructions for Authors (www.plantphysiol.org) is: Erik J. Veneklaas (erik.veneklaas@uwa.edu.au).

H.J.d.B. prepared samples, measured leaf traits, constructed the hydraulics model with input from P.L.D. and E.J.V., analyzed data, and drafted the article; P.L.D. prepared samples, measured leaf traits, derived the photosynthetic parameters, provided input on modeling, analyzed data, and drafted the article; E.J.V. and H.J.d.B. conceived the study and developed it with P.L.D.; E.J.V. oversaw measurements of leaf traits, provided input on modeling, and supervised and complemented the writing; E.W. prepared and measured leaves for vein density and stomatal morphological features; C.A.P. oversaw the vein measurements; E.-D.S. conceived the original sample collection campaigns, measured several leaf traits, and commented on the article; N.C.T. collected the leaf material and commented on the article; D.N. located and identified trees, collected leaves during the sample collection campaigns, and contributed a classification of the eucalypts.

[OPEN] Articles can be viewed without a subscription.

www.plantphysiol.org/cgi/doi/10.1104/pp.16.01313

Considering the dimensions of postvenous water transport led Zwieniecki and Boyce (2014) to hypothesize that a functionally optimal vein placement would be achieved if the average distance between neighboring veins (d_x) is equal to the average distance from veins to the epidermis (d_y), expressed by the ratio d_x:$d_y \approx 1$. This hypothesis is based on modeling and experiments with artificial leaves (Noblin et al., 2008), which suggest that potential maximum transpiration rates increase by increasing vein density when vein densities are relatively low (with d_x:$d_y \gg 1$), whereas potential maximum transpiration rates become independent of vein density when vein densities are very high (with d_x:$d_y \ll 1$). Zwieniecki and Boyce (2014) observed that derived angiosperms achieve an optimal vein architecture (with d_x:$d_y \approx 1$) by combining high vein densities with relatively thin leaves. This specific leaf morphology is unique to angiosperms (Feild et al., 2011; de Boer et al., 2012) and allows high rates of transpiration and photosynthesis, owing to the short distances for postvenous water transport and subsequent high k_{leaf} (Brodribb et al., 2007). Some gymnosperms also achieve optimal vein placement with a contrasting morphology that combines thick leaves with low vein densities, resulting in relatively long postvenous water transport distances and subsequently low k_{leaf}. Deviations from this proposed hydraulically optimal anatomy are observed for fern and basal angiosperm species that, owing to physiological or developmental constraints, underinvest in veins by combining relatively thin leaves with relatively low vein densities, resulting in d_x:$d_y > 1$ (Zwieniecki and Boyce, 2014). This leaf morphology is especially vulnerable to desiccation and, therefore, limited to environments with low light and/or high atmospheric humidity (Feild et al., 2004). Zwieniecki and Boyce (2014) observed few species that overinvest in veins (with d_x:$d_y < 1$) and argue that this leaf hydraulic architecture yields no functional benefit over an optimal vein architecture (d_x:$d_y \approx 1$), because, like the theoretical extreme (d_x:$d_y \ll 1$) exemplified by Noblin et al. (2008), the additional veins may not contribute to additional leaf gas-exchange capacity.

We argue that the proposed optimal leaf hydraulic architecture (d_x:$d_y \approx 1$) may not be the phenotypic end point of evolution in environments that specifically select for traits associated with thick leaves. Thick leaves are most common in warm, arid, and high-light environments because of advantages related to a longer leaf life span (Mott et al., 1982; Niinemets, 2001) and a larger hydraulic and thermal capacitance (Schymanski et al., 2013). Warm and dry climates also select for high vein densities (Sack and Scoffoni, 2013), because this morphology provides greater resistance to loss of k_{leaf} during water stress and may facilitate high photosynthesis rates during (short) wet periods (Grubb, 1998; Scoffoni et al., 2011). The morphological combination of thick leaves (with subsequent long d_y) with high vein densities (with subsequent short d_x) implies that an apparent overinvestment in leaf venation (resulting in d_x:$d_y < 1$) may provide functional benefits under dry and warm climates.

To understand how the selection pressure of aridity shapes leaf form and function, it is important to consider not only the hydraulic aspects of leaf morphological adaptations but also the optimization of photosynthetic biochemistry in relation to the prevailing climate. The fast-slow continuum of the leaf economics spectrum has successfully predicted correlations between photosynthetic capacity, g_s, and leaf nitrogen on the one hand and leaf life span and leaf mass per unit area (LMA) on the other hand (Wright et al., 2004). Although these relationships emerge independent of climate, leaves of drought-adapted plants tend to have a higher LMA and longer life span (Wright et al., 2005). Given the requirement for plants to trade off carbon uptake and water loss, photosynthetic traits also should be coordinated with k_{leaf}. Some empirical evidence for this effect has been presented (Franks, 2006; Sack and Frole, 2006; Brodribb et al., 2007; Brodribb and Jordan, 2008), but a theoretical proposition linking leaf economic traits to these processes (as proposed by Blonder et al. [2011]) has yet to be widely accepted (Sack et al., 2014) or supported experimentally. In contrast to the assertion of coordination, the recent work of Li et al. (2015) indicates a decoupling of leaf economic and leaf hydraulic traits within tropical-subtropical forests. The premise of Li et al. (2015) is that spatial compartmentalization of traits in functionally independent leaf internal structures may enable more nuanced adaptation in habitats that offer a diversity of conditions. Despite potential compartmentalization, leaf hydraulic traits are inherently coupled to leaf economic and photosynthetic traits via constraints imposed by selection for the most productive combinations of leaf life span and leaf morphology (Brodribb et al., 2010). In this way, groups of functionally independent traits are expected to change concurrently to optimize the overall performance of leaves in relation to the environmental pressure of aridity.

We aim to test the hypothesis that coordination between leaf hydraulic and photosynthetic traits is achieved across mesic and arid environments by expressing leaf morphologies that deviate from the theoretical optimal vein architecture with d_x:$d_y \approx 1$, as proposed by Noblin et al. (2008) and Zwieniecki and Boyce (2014), resulting in d_x:$d_y < 1$. Here, we assembled a collection of leaf hydraulic and photosynthetic traits from the closely related genera *Eucalyptus* and *Corymbia* (collectively referred to as eucalypts from here on) that are widely distributed across the mesic-arid spectrum of Australian environments. Fossil evidence suggests that the *Eucalyptus* and *Corymbia* clades evolved from a rainforest precursor during the Paleocene to Early Eocene (Gandolfo et al., 2011). The subsequent diversification and radiation of these genera across continental Australia through the Cenozoic took place against a backdrop of increasing aridity (Ladiges et al., 2003; Martin, 2006). This adaptive radiation required innovations in leaf traits that are manifest in extant species. Work to classify parts of this group using morphological or molecular approaches generally has observed more derived species in arid habitats (Steane et al., 2002, 2011; Hopper, 2003; Ladiges et al., 2003). Within

species, phylogeographical patterns often indicate a complex population structure, indicative of multiple localized refugia associated with historical shifts in aridity (Byrne et al., 2008).

In this study, we draw upon a natural aridity gradient to test whether the leaf hydraulic and photosynthetic traits of eucalypt leaves are coordinated across environments classified by the supply and demand for water. Our analyses expand on the work of Schulze et al. (2006), who sampled eucalypt leaves across a transect that spanned an aridity gradient from the wet coastal region of southwestern Australia to the arid Australian interior near Kata Tjuta. From this collection, we selected three to five leaves per tree from 440 trees, representing 68 species occurring at 73 locations, for analyses of leaf morphological and hydraulic traits along the aridity gradient (Fig. 1; Supplemental Table S1). From this subsample, we selected three leaves from 107 trees (27 species, 30 locations) for measurements of stomatal traits. In our analyses, we specifically focused on the adaptation of the leaf morphological and hydraulic traits that influence the ratio d_x:d_y (Fig. 1). Based on these data sets, we determined the adaptive innovations in leaf morphology and leaf hydraulics that provide specific competitive advantage to eucalypts in arid environments.

RESULTS

Our results show clear differences in eucalypt leaf morphology along an aridity gradient in southwestern Australia. Regression with aridity index (AI) reveals that leaf vein density, expressed as vein length per unit area (VLA), and T_L increase from the mesic to the arid sites ($r^2 = 0.44$, $P < 0.001$ and $r^2 = 0.11$, $P < 0.001$, respectively; Fig. 2). The slopes and intercepts of the models relating VLA to AI (Fig. 2) were not different between hypostomatous and amphistomatous species ($P > 0.05$); hence, a combined model is presented. The increase in T_L with aridity was only significant for amphistomatous leaves and for the combination of amphistomatous and hypostomatous species, and the slopes and intercepts of these models were not significantly different ($P > 0.05$). Although a complete phylogeny for the *Eucalyptus* and *Corymbia* genera is not available, we corrected for the potential effect of sampling bias due to relatedness between species in our sample by resampling several key traits at the taxonomic level of series (a subdivision of genus) using the classification of Nicolle (2015; Supplemental Fig. S5). Our subsequent analysis shows that the relationships between VLA and AI (bootstrapped $r^2 = 0.76$, $P < 0.001$) and between d_x:d_y and AI (bootstrapped $r^2 = 0.67$, $P < 0.001$) are robust to potential sampling bias. The relationship between leaf thickness and AI (bootstrapped $r^2 = 0.2$, $P = 0.16$) is not robust to potential sampling bias, which reflects the weak association between leaf thickness and AI in the raw data, as shown in Figure 2 ($r^2 = 0.11$, $P < 0.001$).

As the leaf veins of the eucalypts studied here are positioned such that there is an equal distance to the

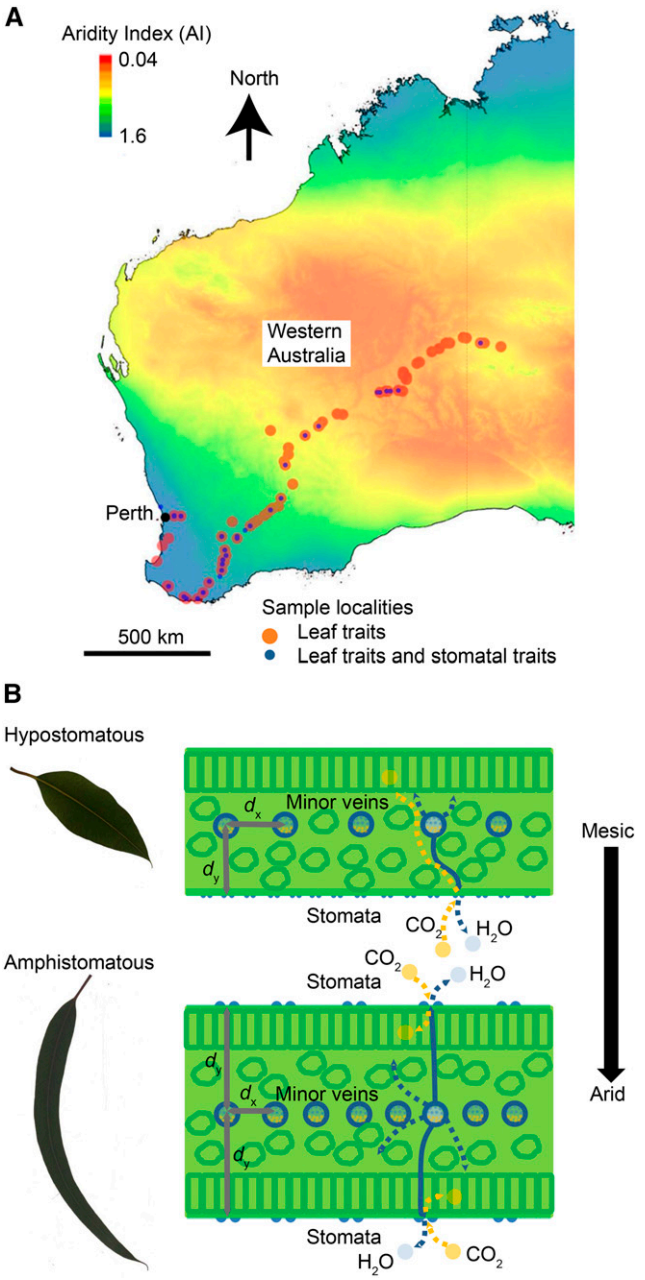

Figure 1. A, Sample localities for *Eucalyptus* and *Corymbia* (referred to as eucalypts) spp. leaves used for measurements of leaf morphological, leaf hydraulic, and stomatal morphological traits. Sampling sites are plotted with the gridded mean annual AI, obtained from the Atlas of Living Australia. B, Schematic cross sections of eucalypt leaf morphologies. The hypostomatous leaf type is most common in mesic environments and characterized by the presence of stomata only on the abaxial surface and palisade mesophyll toward the adaxial surface. The amphistomatous leaf type is most common in arid environments and characterized by the presence of stomata on both abaxial and adaxial surfaces and palisade mesophyll toward both abaxial and adaxial surfaces. The differences in terms of d_x and d_y between the hypostomatous and amphistomatous leaf morphologies are indicated. The blue and yellow lines depict the pathway for water and CO_2 transport, respectively, as a liquid (solid lines) and a gas (dashed lines).

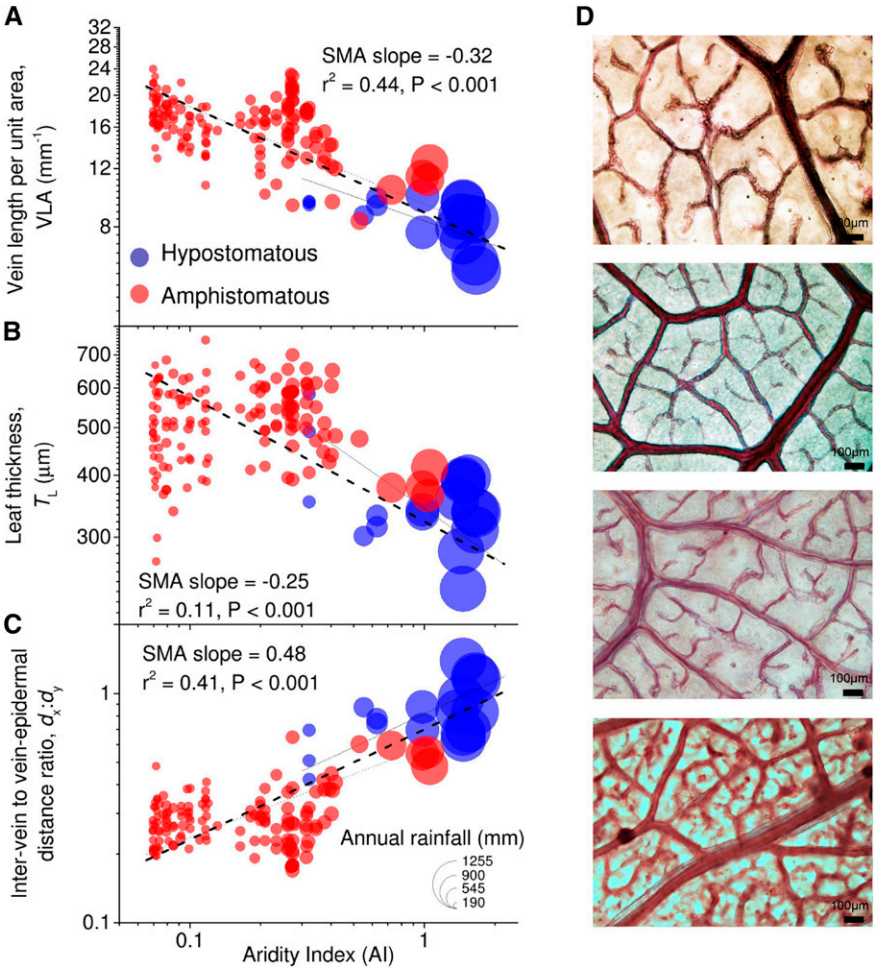

Figure 2. A to C, Correlations between the mean annual AI and VLA (A), T_L (B), and d_x:d_y (C). The color indicates stomatal distribution (hypostomatous or amphistomatous). The diameter of the symbols is proportional to the AI of the sampling locations. Fitted lines are standardized major axis (SMA) regression models with slope, r^2, and significance of the models fitted across all data indicated. Thin solid and dashed lines are, respectively, the significant models for hypostomatous and amphistomatous species, with the thick dashed lines representing the model fitted to all data. D, Paradermal view of cleared and stained eucalypt species leaves. Species shown from top to bottom are *E. jacksonii* (sample VLA = 8 mm mm^{-2}), *E. marginata* (sample VLA = 11 mm mm^{-2}), *E. wandoo* (sample VLA = 13 mm mm^{-2}), and *E. salmonophloia* (sample VLA = 24 mm mm^{-2}). High-resolution images of these and an additional four samples are included as supplemental material.

upper and lower epidermis (Supplemental Fig. S1; Supplemental Table S2), increases in T_L are proportional to increases in d_y. Furthermore, increases in VLA are closely linked to decreases in d_x ($r^2 = 1$, $P < 0.001$; Supplemental Fig. S2). Hence, the observed d_x:d_y ratios decrease along the aridity gradient as a result of the combined increases in VLA and T_L from mesic to arid sites ($r^2 = 0.41$, $P < 0.001$; Fig. 2). This pattern was evident regardless of stomatal distribution, and the slopes and intercepts of the models describing these relationships did not differ significantly between hypostomatous and amphistomatous species ($P > 0.05$). In our sample of eucalypts, the d_x:d_y ratios range between 0.15 and 1.6 and, thereby, extend notably below the proposed theoretical optimum ratio d_x:$d_y \approx 1$. Our results also reveal a shift from a hypostomatous to amphistomatous leaf morphology toward the more arid sites. Consequently, the amphistomatous species in our data set have leaves with a higher VLA than the hypostomatous species (16 ± 3.7 and 9 ± 2.1 mm mm^{-2}, respectively; $P < 0.001$) and a larger T_L (517 ± 97 and 350 ± 75 μm, respectively; $P < 0.001$). These morphological contrasts manifest as a lower d_x:d_y in amphistomatous species compared with hypostomatous species (0.3 ± 0.1 and 0.82 ± 0.24, respectively; $P < 0.001$; Supplemental Fig. S3). Our species level comparison of d_x:d_y also reveals that both the hypostomatous and amphistomatous eucalypts differ from the derived angiosperms of Zwieniecki and Boyce (2014; Supplemental Fig. S3). Only the amphistomatous eucalypts differ significantly from the proposed 1:1 ratio as hypothesized by Noblin et al. (2008). We note that our measurements of these leaf morphological and hydraulic traits were performed on rehydrated leaves that had been stored after drying. Our analyses to quantify the potential error arising from this approach indicate that leaf area and T_L, affecting d_x and d_y, respectively, may have been underestimated by 2.2% ± 2.7% and 8.9% ± 4.2%, respectively (Supplemental Fig. S4). As the reduction in T_L is larger than the reduction in leaf area, we argue that the reported values of d_x:d_y may be overestimated by approximately 5% to 10%.

A principal component analysis (PCA) of the leaf morphological data set indicates the coupling of hydraulic and photosynthetic traits (Fig. 3). The PC1 axis accounts for 59% of the variation, and this is dominated by loadings on d_x:d_y, LMA, L_T, and k_{leaf}. For PC2, which accounts for 17% of the variation, strong loadings are evident on the V_{cmax}, VLA, and k_{leaf}. The PCA scores

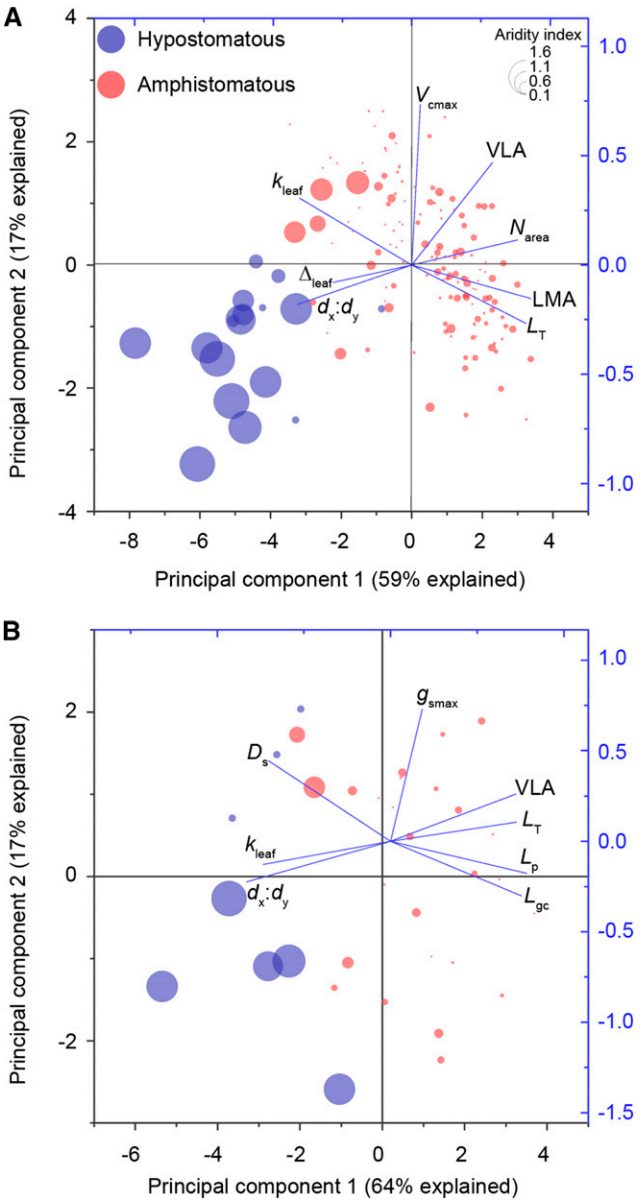

Figure 3. PCA of leaf hydraulic and leaf morphological traits (A) and leaf hydraulic, leaf morphological, and stomatal morphological traits (B). Trait loadings are indicated as blue lines, and trait abbreviations are provided in Tables I and II. Additional traits not mentioned in these tables are the maximum carboxylation rate (V_{cmax}) and the k_{leaf}. The diameter of the symbols is proportional to the AI of the sampling locations, and the color indicates the stomatal distribution (hypostomatous versus amphistomatous).

show clear separation in relation to aridity and stomatal distribution, which highlights the dominant effect of aridity on leaf morphology within the eucalypts studied here. A PCA of the stomatal morphological data set also displays the coupling of hydraulic and photosynthetic traits (Fig. 3). The PC1 axis accounts for 64% of the variation and is dominated by loadings on d_x:d_y, stomatal pore length (L_p), guard cell length (L_{gc}), and VLA. The PC2 axis accounts for 17% of the variation and is dominated by loadings on the anatomical maximum stomatal conductance to water vapor (g_{smax}) and stomatal density (D_S). As with the leaf morphological data set, separation in relation to aridity and stomatal distribution is evident.

Linear regression statistics further support the PCA-derived coupling of hydraulic and photosynthetic traits in both the leaf morphological and stomatal data sets (Tables I and II, respectively). In relation to our hypothesis, the leaf morphological data set reveals a close association between the ratio d_x:d_y and a variety of leaf traits that span the hydraulic and photosynthetic categories. Crucially, d_x:d_y is negatively correlated with LMA ($r^2 = 0.57$, $P < 0.001$) and leaf nitrogen per unit area (N_{area}; $r^2 = 0.42$, $P < 0.001$), whereas both LMA and N_{area} are negatively correlated with the leaf carbon isotope ratio (Δ_{leaf}; $r^2 = 0.34$, $P < 0.001$ and $r^2 = 0.35$, $P < 0.001$, respectively; Table I). The stomatal data set reveals a close association between leaf hydraulic traits and stomatal morphology. Here, d_x:d_y is positively correlated with both guard cell length and stomatal pore length ($r^2 = 0.44$, $P < 0.001$ and $r^2 = 0.52$, $P < 0.001$, respectively; Table II).

The leaf morphologies of the eucalypts studied here deviate from the analysis of Zwieniecki and Boyce (2014), which shows that derived angiosperms closely coordinate d_x with d_y via changes in VLA and the lateral position of veins inside the leaf to achieve d_x:d_y ratios near unity (Fig. 4). Unlike the relationship reported by Zwieniecki and Boyce (2014), our linear regression model describing variation in d_x based solely on d_y gives only a weak fit (correlation $r^2 = 0.16$, $P < 0.001$ in Fig. 4 and adjusted $r^2 = 0.15$, $P < 0.001$ in Supplemental Table S3 for the regression model). The inclusion of AI in a multiple regression model substantially improves the model fit (adjusted $r^2 = 0.51$, $P < 0.001$; Supplemental Table S3). In spite of this result, the close relationship between aridity and the shift from hypostomaty to amphistomaty (Supplemental Fig. S3) restricts our ability to statistically resolve the underlying cause for a negative relationship between d_x and d_y in our eucalypt sample. Still, our observation that the relationship between d_x:d_y and AI is comparable across hypostomatous and amphistomatous eucalypt species-site combinations (Fig. 2) suggests that aridity shapes the negative relationship between d_x and d_y and that amphistomaty is a separate adaptation that also is associated with aridity.

The low values of d_x:d_y observed in our selection of eucalypts are a result of the combined increases in T_L and VLA along the aridity gradient. We hypothesized that these adaptations reflect the selection pressure of aridity on leaf morphology, whereby increases in leaf thickness and LMA result from selection for a longer leaf life span, while the increases in VLA occur from selection for enhanced water supply and the need to compensate for the potential loss in photosynthesis owing to the increase in leaf thickness. This hypothesis is supported by our within-site comparisons of species-level differences in T_L, d_x:d_y, $\bar{A}$, and VLA relative to

differences in LMA (Fig. 4). The comparisons show that, within sites, species with a higher LMA have, on average, thicker leaves ($P < 0.001$, $n = 128$) with lower d_x:d_y ($P < 0.01$, $n = 128$) than species with lower LMA. Cooccurring species with higher LMA also have lower $\bar{A}$ than species with lower LMA ($P < 0.001$, $n = 178$). In contrast to the correlation between LMA and VLA that we observed across sites ($r^2 = 0.22$, $P < 0.001$; Table I), we found no within-site difference in VLA between species with different LMA ($P > 0.05$, $n = 178$; Fig. 4). This result suggests that the key hydraulic trait VLA may be decoupled from LMA within sites, despite their correlated adaptation to the common selection pressure of aridity across the sampled sites.

The observation that our sample of eucalypts includes many species with d_x:d_y ratios below unity raises the question of the extent to which this leaf morphology conveys an advantage in terms of additional gas exchange in comparison with a leaf morphology with d_x:$d_y \approx 1$. As the observed adaptations in d_x:d_y are closely linked to the photosynthetic and stomatal traits considered here (Tables I and II), our empirical data cannot be used to directly test our hypothesis that these adaptations provide an advantage in terms of additional transpiration and photosynthesis. Therefore, we used the semiempirical leaf hydraulic model of Brodribb et al. (2007) and Brodribb and Feild (2010) to determine how changes in hydraulic architecture influence leaf gas exchange. We quantified the potential gas-exchange advantage of reducing d_x:d_y below unity in terms of the modeled difference in Rubisco-limited photosynthesis between the observed leaf morphology and a leaf morphology with d_x:$d_y = 1$ as the percentage difference, termed δA, for all species-site combinations. This model approach is explained in detail in "Materials and Methods." A sensitivity and uncertainty analysis of the model is provided in Supplemental Figures S7 and S8. Our model results show that the observed reduction in d_x:d_y below unity reduces l_{H2O} and thereby increases the modeled k_{leaf} (Fig. 5). This effect is most pronounced in thick leaves, which suffer most from reduced k_{leaf} when the theoretical optimal hydraulic architecture d_x:$d_y \approx 1$ is maintained. Our modeling results show that the reductions in d_x:d_y below unity provide a small but significant photosynthetic advantage δA of 8.1% ± 3.4% across all our species-site combinations (Fig. 5). The group of amphistomatous species shows a larger average photosynthetic advantage of reducing d_x:d_y below unity than the group of hypostomatous species, with $\delta A = 8.9\% \pm 2.5\%$ for the amphistomatous species and $\delta A = 1.2\% \pm 1.6\%$ for the hypostomatous species.

DISCUSSION

Our results reveal that, in eucalypts, high vein densities occur in thick and amphistomatous leaves, especially in species growing in the most arid localities. The consequence of this leaf morphology is that the observed range in the ratio between the intervein distance d_x and the vein-epidermal distance d_y extends to well below the proposed theoretical optimal ratio d_x:$d_y \approx 1$ (Noblin et al., 2008). Eucalypts thus form an exception to the strong 1:1 relationship reported for other derived angiosperm species (Zwieniecki and Boyce, 2014).

Theoretical optimal vein placement requires close coordination between leaf vein density, the position of veins in the leaf, and leaf thickness that inadvertently requires leaves with highest k_{leaf} to be relatively thin. However, arid environments select for thicker leaves owing to their longer life span (Wright and Westoby, 2002), larger thermal and hydraulic capacitance (Schymanski et al., 2013), and limited palatability (Chabot and Hicks, 1982; Choong et al., 1992). The result of selection for thicker leaves is a larger vein-epidermal distance d_y and, all else being equal, a decrease in k_{leaf} and photosynthesis. Crucial is that a decrease in k_{leaf} limits maximum rates of photosynthesis because it pertains directly to leaf water status and the control of g_s. As water may be available during short intervals in arid environments, there may be strong selection pressure for a higher k_{leaf} (Grubb, 1998; Scoffoni et al., 2011). However, owing to the selection pressure for thicker leaves in arid environments, the remaining option to increase k_{leaf} is to increase vein density and, subsequently, reduce the ratio d_x:d_y. The coincidence of thick leaves and high vein densities in our study, therefore, does not point to a mechanistic coordination of these traits, as discussed between Blonder and Enquist (2014) and Sack et al. (2014), but rather to parallel selection driven by common selection pressures associated with aridity.

The VLA observed in our sample of eucalypts ranges from 6 mm mm^{-2} in relatively mesic sites up to 24 mm mm^{-2} in the most arid localities. Our measurements

Table I. *Standardized major axis linear regression results of functional traits from all sampled leaves*

***, $P < 0.001$. r^2 values are shown in the bottom half of the table. +, Positive correlation; −, negative correlation. Data were log transformed prior to analysis.

Trait	Abbreviation	VLA	d_x:d_y	N_{area}	Δ_{leaf}	LMA	L_T
Vein density	VLA	–	***	***	***	***	***
Ratio of intervein to vein-epidermis distance	d_x:d_y	0.76 (−)	–	***	***	***	***
Area-based nitrogen concentration	N_{area}	0.17 (+)	0.42 (−)	–	***	***	***
Leaf carbon isotope fractionation	Δ_{leaf}	0.10 (−)	0.18 (+)	0.35 (−)	–	***	***
Leaf dry mass per area	LMA	0.22 (+)	0.57 (−)	0.63 (+)	0.34 (−)	–	***
Leaf thickness	L_T	0.13 (+)	0.58 (−)	0.44 (+)	0.14 (−)	0.73 (+)	–

Table II. *Standardized major axis linear regression results of functional traits from leaves sampled for stomatal morphology*

NS, $P > 0.05$; *, $P < 0.05$; **, $P < 0.01$; and ***, $P < 0.001$. r^2 values are shown in the bottom half of the table. + Positive correlation; − negative correlation. Data were log transformed prior to analysis.

Trait	Abbreviation	VLA	d_x:d_y	L_{gc}	L_p	D_S	g_{smax}	L_T
Vein density	VLA	–	***	***	***	*	**	**
Ratio of intervein to vein-epidermis distance	d_x:d_y	0.81 (−)	–	***	***	*	*	***
Guard cell length	L_{gc}	0.33 (+)	0.44 (−)	–	***	***	NS	***
Stomatal pore length	L_p	0.49 (+)	0.52 (−)	0.80 (+)	–	***	NS	***
Stomatal density	D_S	0.13 (−)	0.12 (+)	0.57 (−)	0.60 (−)	–	**	NS
Anatomical maximum stomatal conductance	g_{smax}	0.20 (+)	0.12 (−)	0.00	0.03	0.14 (+)	–	NS
Leaf thickness	L_T	0.26 (+)	0.68 (−)	0.32 (+)	0.29 (+)	0.06	0.01	–

of VLA are slightly overestimated, as our analyses were performed on rehydrated leaves, which revealed an average shrinkage of 2.2% ± 2.7% compared with fresh leaves (Supplemental Fig. S4). This effect is of similar magnitude to the shrinkage reported in rehydrated leaves by Blonder et al. (2012). Our observation that VLA in eucalypts increases with increasing aridity is in line with the global compilation of vein density data by Sack and Scoffoni (2013), who show a strong correlation between VLA and aridity across biomes. Their review includes only two eucalypt species (*Eucalyptus hemastoma* and *Eucalyptus globulus* with VLA of 4.1 and 7.4 mm mm^{-2}, respectively), which are from relatively mesic habitats and have vein densities comparable to our mesic species-site combinations. The upper end of the vein density range of our eucalypt sample overlaps the highest vein densities of evergreen shrubs and trees reported by Sack and Scoffoni (2013). Boyce et al. (2009) observed that these high vein densities (greater than 20 mm mm^{-2}) occur only in the rosid clade, which *Eucalyptus* and *Corymbia* belong to. Hence, this phylogenetic background may have allowed eucalypts to develop the specific leaf morphology that combines relatively thick leaves with high vein densities.

Mitigating the effect of leaf thickness on k_{leaf} by adjusting VLA and subsequent d_x:d_y may be critical for species in arid environments that must maximize carbon gain during short pulses of high soil moisture content (Sack and Scoffoni, 2013). This growth strategy likely became relevant during the evolution of eucalypts, because major differentiation of the *Eucalyptus* and *Corymbia* clades took place during a transition to greater aridity (Ladiges et al., 2003). This climatic shift provided ecological opportunities, but the ensuing adaptive radiation of species formerly suited to rainforests, the precursors of modern eucalypts, would have occurred in an environment increasingly characterized by long dry periods punctuated by brief wet episodes (Martin, 2006). These novel environments ultimately would have encouraged the convergence of traits enabling a long leaf life span and high thermal capacitance with traits supporting higher rates of leaf water transport and photosynthesis (Givnish et al., 2005). Leaves would necessarily become thicker, but at the same time selection for maximum photosynthetic yield would lead to the evolution of higher vein densities. Zwieniecki and Boyce (2014) suggest that such an overinvestment in veins may result in a decrease in photosynthetic capacity due to a loss of internal space that could be allocated to chlorophyll-bearing cells. However, in thick amphistomatous leaves of (semi)arid biomes, photosynthetic capacity may not be limited by space constraints but, rather, by the ability of the hydraulic network to sustain liquid and vapor water transport.

Although the influence of adjusting intervein distance d_x on k_{leaf} is less than the effect of adjusting vein-epidermal distance d_y (Noblin et al., 2008), our modeling results indicate that the eucalypts studied here may still gain a small but significant photosynthetic benefit of reducing d_x:d_y below unity. Our model is based on the empirical relationship between k_{leaf} and l_{H2O} found by Brodribb et al. (2007). This relationship highlights that the water transport pathway outside the xylem is the major constraint to k_{leaf} (Sack and Scoffoni, 2013; Buckley et al., 2015). According to our model, the photosynthetic advantage increases with decreasing d_x:d_y further below unity. Hence, the combined adaptation of increasing leaf thickness and increasing VLA could have provided an evolutionary advantage in terms of additional productivity during (short) periods with sufficient water. As our measurements of d_x:d_y may be overestimated owing to the use of dried and rehydrated laves, the modeled advantage could be slightly underestimated. Still, our interpretation of the modeling results appears at odds with the conclusion of Zwieniecki and Boyce (2014) and the results from artificial leaves of Noblin et al. (2008), who suggest that additional leaf veins do not contribute to additional leaf gas exchange in the theoretical extreme situation with d_x:$d_y \ll 1$. However, the modeling results of Noblin et al. (2008) also suggest that d_x:d_y can extend to below unity before the response of increasing transpiration rate with increasing vein density fully saturates, and this is especially so when the vein-epidermal distance is relatively large and vein diameters are small. This interpretation of Noblin et al. (2008) is consistent with our observations on eucalypt leaf morphology, which shows that the lowest d_x:d_y ratios occur in the thickest leaves with the highest vein densities. Therefore, we argue for a more nuanced interpretation of the ratio d_x:d_y by considering the specific growth environments and leaf morphologies, in

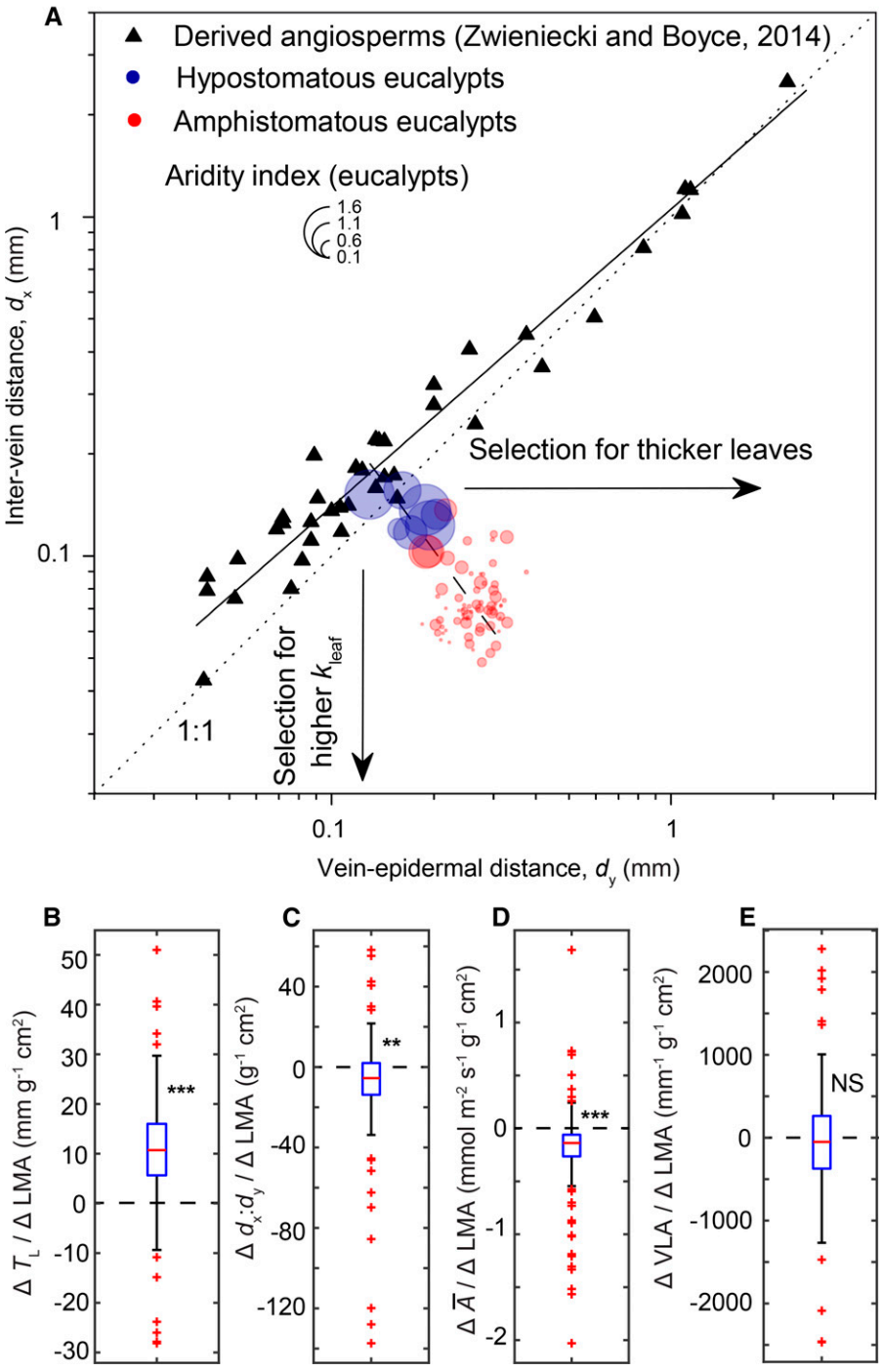

Figure 4. Across-site and within-site relationships between leaf morphological and leaf hydraulic traits. A, Observed adaptation of d_x and d_y away from the proposed optimal ratio d_x:$d_y \approx 1$ across the sampled aridity gradient. Derived angiosperm data are from Zwieniecki and Boyce (2014). r^2 = 0.95, $P < 0.001$, and SMA slope = 0.88 for derived angiosperms and r^2 = 0.16, $P <$ 0.001, and SMA slope = −1.37 for eucalypts. The eucalypt sample represents species averages. B to E, Within-site difference (Δ) between species, reflecting the difference in T_L relative to LMA (ΔT_L/ΔLMA [n = 128]; B), the difference in d_x:d_y relative to LMA (Δd_x:d_y/ΔLMA [n = 128]; C), the difference in time-integrated photosynthesis ($\bar{A}$) relative to LMA ($\Delta\bar{A}$/ΔLMA [n = 178]; D), and the difference in VLA relative to LMA (ΔVLA/ΔLMA [n = 178]; E). The central mark in the box plots indicates the median, the edges of the box are the 25th and 75th percentiles, and the whiskers cover 2.7 SD. Points outside the whiskers are plotted individually. Significant deviation of the population means from zero is indicated as NS for $P > 0.05$, ** for $P <$ 0.01, and *** for $P < 0.001$.

which small increments in leaf gas exchange may yield specific competitive advantages.

Our results also reveal that various leaf morphologies coexist in the same site and that thicker leaves with a lower d_x:d_y do not offer an absolute competitive advantage compared with thinner leaves with a higher d_x:d_y. These within-site variations in d_x:d_y and T_L could reflect the exploitation of different niches, as proposed by Li et al. (2015) drawing on observations from a structurally complex (sub)tropical environment, where light limitation is an important selection pressure. For the eucalypts in our study, where light is not limiting, niche differentiation is likely to manifest as different rooting depths and soil preferences (Drake et al., 2011; Poot and Veneklaas, 2013), resulting in differences in water availability, which in turn will influence stomatal opening and carbon gain over the life span of a leaf. Thus, species with thick leaves may cooccur with thin-leafed

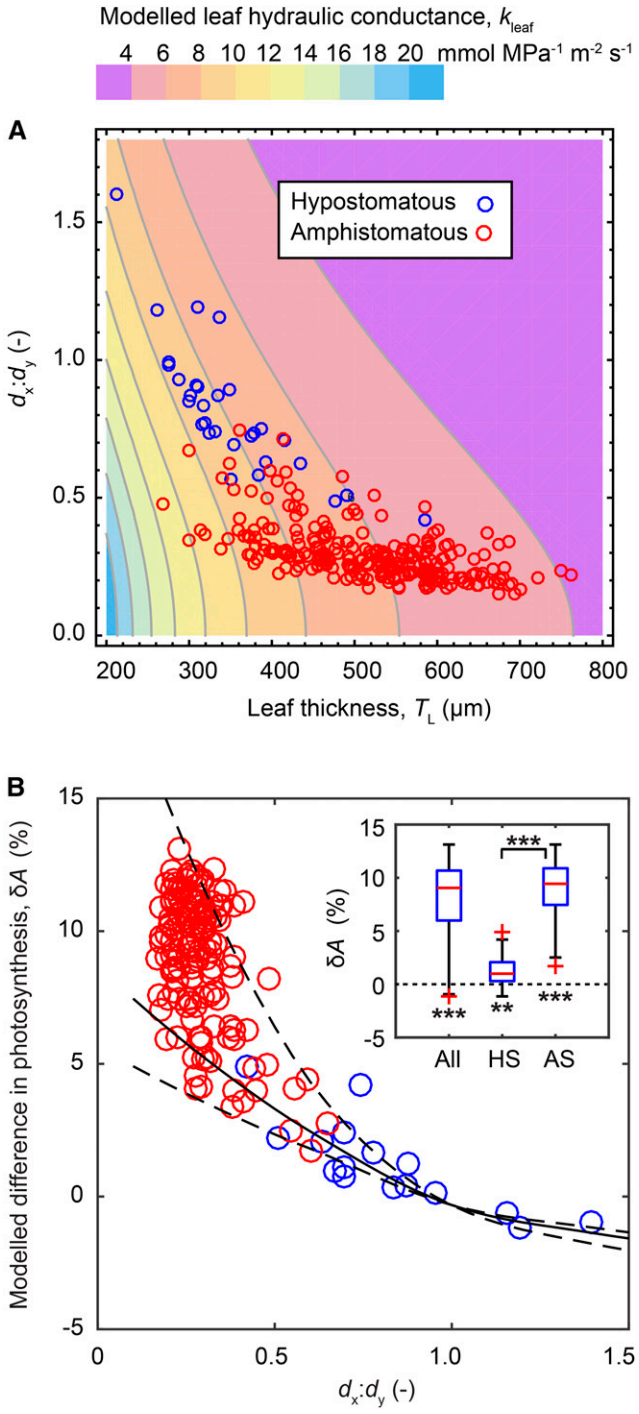

Figure 5. Leaf gas exchange advantage of apparent overinvestment in leaf venation. A, Effects of leaf morphological changes in d_x:d_y and T_L on modeled k_{leaf}. Blue and red circles show leaf morphologies observed for the hypostomatous and amphistomatous eucalypts, respectively. B, Modeled difference in photosynthesis (δA [%]) of the observed leaf morphologies relative to the theoretical optimal leaf morphology with d_x:d_y = 1 plotted as a function of the observed d_x:d_y. Blue and red circles are as in A. The black line shows the modeled δA for parameter values averaged across all species and sites. Dashed black lines show the 1σ confidence interval for modeled δA using the observed range in T_L as input variability. The inset shows distributions of δA (%) modeled for combinations of all sites and all species (n = 159), hypostomatous (HS) species-site combinations only (n = 17), and amphistomatous (AS) species-site combinations only (n = 142). The central mark in the box plots indicates the median, the edges of the box are the 25th and 75th percentiles, and the whiskers cover 2.7 SD. Points outside the whiskers are plotted individually. The significance of the difference between the population means and zero, and between the hypostomatous and amphistomatous population means, are indicated as ** for $P < 0.01$ and *** for $P < 0.001$.

species due to morphological specialization to specific niches in relation to leaf economic tradeoffs.

A specific additional benefit of high VLA in arid environments also may lie in the selection for longer-lived leaves (Wright and Westoby, 2002) as leaf aging will inevitably lead to some loss of hydraulic continuity when the cumulative exposure to water stress increases. The vascular redundancy of leaves with high vein densities of a reticulate nature may reduce the risk of complete hydraulic failure under these circumstances (Scoffoni et al., 2011; Price and Weitz, 2014) by providing alternative parallel flow paths for water transport (Sack et al., 2008). Thus, selection for elevated vein densities in arid biomes may occur both to mitigate the effect of leaf thickness and to reduce the risk of hydraulic failure due to water stress. Although our observations are limited to the eucalypt group, we expect that similar morphological trends may be present in other (semi)arid evergreens.

Our results confirm the well-known link between leaf thickness, aridity, and amphistomaty (Mott et al., 1982), as thicker amphistomatous leaves were found more commonly in eucalypts growing in the most arid environments. Amphistomaty has different implications for the leaf internal conductance of water (liquid or vapor) than for the leaf internal conductance of CO_2. Our results indicate that amphistomaty does not reduce the path length from vein to stomata, as both hypostomatous and amphistomatous leaves have their veins at approximately mid depth. However, amphistomaty does reduce the average path length for CO_2 diffusion to the mesophyll in thick leaves. Although other factors, including mesophyll cell surface area, cell wall thickness, and chloroplast distribution also are strong determinants of mesophyll conductance to CO_2 (Flexas et al., 2013), it would seem that amphistomaty tends to favor water use efficiency due to a larger positive effect on CO_2 conductance than hydraulic conductance. Hypostomatous leaves are more common at mesic locations in our study, where leaves also are thinner. The shorter pathways for water and CO_2 transport in thin leaves of mesic environments may favor the presence of stomata solely on the abaxial surface (de Boer et al., 2012). The close relationship between aridity and stomatal distribution challenges our ability to disentangle the effect of leaf type versus the specific adaption of leaf morphology to aridity as an underlying cause for the negative relationship between d_x and d_y. Although we infer that aridity shapes this relationship in eucalypts,

further work focusing on thick hypostomatous leaves of arid environments would offer additional insight.

The observed adaptations in leaf morphology described here create a more complete picture of eucalypt adaptations to their environments. Of particular interest is the fact that the high-LMA amphistomatous leaves of (semi)arid habitats tend to have nearly vertical angles. High leaf mass may contribute to that trait, but the nearly vertical leaf angle in eucalypts is generally interpreted as enabling greater carbon capture when the sun is at low angles and temperature and vapor pressure deficit are lower (King, 1997). At such steep leaf angles, the amphistomatous and isobilateral form (Gillison, 1981) presumably enables light entry into the leaf from either or both sides. In contrast, in mesic environments, vegetation tends to have higher leaf area indices, and most light enters leaves from above (i.e. from the adaxial surface of the hypostomatous leaves that are common in such environments). Thinner and less dense leaves (with lower LMA) tend to have a higher photosynthetic light use efficiency than thicker and denser leaves (Reich et al., 1992; Niinemets, 2001). In arid habitats, where light is not limiting (Bloom et al., 1985), the selection pressure for high light use efficiency is presumably weak. Hence, the relatively thick eucalypt leaves of (semi)arid habitats may confer little, if any, negative consequences for photosynthesis, due to relaxation of the morphological constraints on leaf venation.

CONCLUSION

We conclude that arid environments select for thicker amphistomatous leaves in eucalypts. Thick leaves challenge the underlying selective pressure to distribute water efficiently to the sites of evaporation because their morphology increases the distance for vein-to-stomata transport. To some extent, eucalypts have overcome this problem by developing leaves with a high vein density, thereby reducing the intervein distance. In this way, deviation from the theoretical optimal vein placement can be considered a response to the selective advantage of producing thick leaves in arid environments.

MATERIALS AND METHODS

Plant Material

In 2003 and 2004, leaves of *Eucalyptus* spp. and closely related *Corymbia* spp. were sampled from 971 trees of 68 distinct species across a transect that spanned 73 locations along an aridity gradient from the wet coastal region of southwestern Australia to the arid Australian interior near Kata Tjuta (Schulze et al., 2006). From this collection, we selected three to five leaves per tree from a total of 440 trees, representing all species and all locations of the original data set for analyses of leaf morphological traits along the aridity gradient (Fig. 1; Supplemental Table S1). From this subsample, we selected three leaves from 107 trees (27 species, 30 locations) for measurements of stomatal traits. Our analyses were performed at the species-by-site level. This approach allows for genetic and phenotypic differences to influence the observed relationships with aridity. We deviate from this approach when analyzing the relationship between d_x and d_y, where we aggregate our data to the species level to match the data of Zwieniecki and Boyce (2014). To compare the sensitivity of these different averaging approaches, we analyzed two critical results: the relationship d_x and d_y and the relationship between the d_x:d_y ratio and AI for our eucalypt sample at both levels of averaging (Supplemental Table S3).

Climate Variables

Climate variables for each location were obtained from the Atlas of Living Australia, a repository for large environmental and ecological data sets (http://www.ala.org.au; accessed December 15, 2015). We selected the climatological variables that were representative of gridded data at a resolution of approximately 1 km. We integrate water supply and demand for each location as annual AI, the average of monthly ratios of precipitation to potential evaporation (pan, free-water surface). This is an adaptation of the index proposed by the United Nations Environmental Program and cited by Middleton and Thomas (1997). Additional climate variables obtained from this repository were mean annual daytime vapor pressure deficit, mean annual daytime temperature, and mean annual rainfall. We are aware that these climate variables, while representative of long-term trends, may not reflect the exact conditions under which individual leaves developed. However, as the emphasis of our study is to demonstrate and interpret leaf morphological changes along an aridity gradient rather than to study the relationships between climate variables and water relations of individual leaves, we argue that the climate data provide sufficient detail for our analyses.

Leaf Morphological Traits

Fresh leaf area, leaf dry weight, and LMA (g cm^{-2}) were determined for three to five leaves from each of the 440 trees sampled in this study. To determine T_L (μm), we randomly selected one leaf per tree ($n = 270$ trees of the 68 species) and cut out a 1-cm^2 fragment at approximately the mid point of the leaf long axis. Since the leaves had been oven dried, these subsamples were first immersed in dilute detergent for 1 h to soften the highly sclerophyllous tissue. Cross sections were then taken from each subsample using a microtome set to a thickness of 15 μm. The cross sections were stained in 5% Toluidine Blue for 10 s, rinsed in deionized water, and then mounted on clear microscope slides using Kaiser's jelly: 1:5:4:1 gelatin:glycerol:water:antibacterial solution (Listerine). We measured T_L at 100× magnification using a compound light microscope (BX51; Olympus), with $n = 3$ measurements for each cross section. The presence of stomata on either the abaxial surface (hypostomatous) or both the abaxial and adaxial surfaces (amphistomatous) was determined during these microscopic analyses for all the species considered. The error in T_L resulting from the use of dried and rehydrated leaves was quantified on a set of fresh eucalypt leaves, which revealed an 8.9% ± 4.2% residual reduction in T_L (Supplemental Fig. S4). The vein-epidermis distance (d_y [μm]) was derived from leaf thickness as $T_L/2$. This simplification was justified by regression analyses of the relationship between d_y and $T_L/2$ from cross sections of a random selection of 43 species ($r^2 = 1$, $P < 0.001$, $n = 111$ leaves; Supplemental Data S1; Supplemental Fig. S1; Supplemental Table S2). For this sample, d_y was measured with respect to the abaxial (lower) epidermis.

Leaf Venation Traits

The leaf vein density was expressed as VLA (mm mm^{-2}) and measured by sampling 1- to 2-cm^2 sections from three leaves per tree from each of the 440 trees at approximately the mid point of the long axis while avoiding the mid rib. The sample was placed in a 5% sodium hydroxide solution until the cuticle had dissolved to reveal the vein network (2–3 weeks; Brodribb and Feild, 2010; Sommerville et al., 2012). The samples were then rinsed in deionized water, stained in a solution of safranin in 5% ethanol for 1 h, and then rinsed in deionized water. Three images of each leaf were then obtained using a dissecting microscope (model SMZ800; Nikon Instrument) at 40× magnification, and the vein network was traced by hand using Paint (Microsoft). In light of the high VLA values of our collection, we confirmed that the minor veins of cleared leaves were conductive by drawing dye through fresh leaves via transpiration and observing the vein network from paradermal images (Supplemental Fig. S6, A and B). A leaf cross section also is presented to confirm the positions of these numerous small veins as well as the presence of several small chlorenchyma cells in the mesophyll tissue of the intervein space (Supplemental Fig. S6C). Also, we quantified the amount of leaf shrinkage from drying and the subsequent expansion after rehydration on a set of fresh eucalypt leaves, which revealed a 2.2% ± 2.7% residual reduction in leaf area (Supplemental Fig. S4).

The traced vein network of each image was analyzed further in Matlab (version R2015b). The average VLA of each traced image was obtained

following Blonder et al. (2011). First, each set of traces was smoothed and reduced to the width of a single pixel using the skeletonizing algorithm of the function bwmorph. Total vein length was calculated from the skeletonized vein network using the function bwarea. The VLA was calculated as the quotient of total vein length and total image area.

The intervein distance (d_x [μm]) was obtained from the skeletonized vein network images by automatically drawing 10,000 random cross sections across each traced image. For each cross section, we mapped the points where the cross section intersected with a traced vein and subsequently calculated the average distance between the veins in each cross section. This automated method resembles the manual cross-section approaches of Blonder and Enquist (2014) and Zwieniecki and Boyce (2014). The grand mean distance between veins in all randomly drawn cross sections was then calculated per image to obtain an average d_x for each sampled leaf.

Stomatal Morphological Traits

Three leaves were selected for each of the 27 species chosen for the determination of stomatal traits. For each leaf, a 1-cm^2 section was sampled and placed into a 2-mL Eppendorf tube. Each tube received a 1:1 solution of 80% ethanol and 30% hydrogen peroxide. The tubes were left unsealed and placed into a water bath set at 60°C until the cuticles and epidermis began to detach from the underlying mesophyll and vascular tissues (after approximately 48 h). The samples were then removed from the tubes and rinsed under tap water. The cuticle and epidermis of both the abaxial and adaxial surfaces were then carefully detached from the remaining tissue with fine forceps, stained in 5% safranin for 30 s, and then rinsed in deionized water. The peels were then transferred to microscope slides and mounted using Kaiser's jelly. D_S (mm^{-2}; i.e. number of stomata per unit epidermal area) was calculated for each stomata-bearing leaf surface as the mean of five fields of view at 400× magnification using a compound light microscope (BX51; Olympus). Stomatal morphological parameters were measured as the mean of 20 stomatal complexes (guard cell pairs) for each stomata-bearing surface at 1,000× magnification using the same light microscope. Stomatal morphological parameters were L_{gc} (μm), guard cell width (W_{gc} [μm]), and L_p (μm; Franks et al., 2009). The g_{smax} (mol m^{-2} s^{-1}) of the stomata-bearing leaf surface was estimated according to Franks and Farquhar (2001) and Franks et al. (2009):

$$g_{s\max} = \frac{D_S d a'}{V\left(l + \frac{\pi}{2}\sqrt{\frac{a'}{\pi}}\right)} \quad (1)$$

where d is the diffusivity of water in air (m^2 s^{-1}), a' is the mean maximum stomatal pore area (m^{-2}), which was estimated as $L_p^2 \times \pi/4$, V is the molar volume of air (m^3 mol^{-1}), and l is the depth of the stomatal pore (m), which was assumed to be equal to W_{gc}. For hypostomatous leaves, the estimate of g_{smax} is based on the stomatal morphology of a single leaf side, whereas g_{smax} for amphistomatous leaves is the sum of both leaf surfaces based on the assumption that gas exchange from the abaxial and adaxial surfaces occurs in parallel.

Leaf Nitrogen and Leaf Carbon Isotopic Composition

Schulze et al. (2006) collected a subsample of oven-dried leaves from each of the 440 trees. The leaves were finely ground, and part of this material was used to determine total leaf nitrogen (% by mass) using a nitrogen analyzer (Vario EL II; Elementar). Leaf nitrogen as a percentage of mass (N_{mass}) was converted to an area basis as N_{area} (g cm^{-2}) = N_{mass} (%) × LMA × 100. The leaf carbon isotope ratio ($\delta^{13}C_{leaf}$) of the remaining ground material was determined following combustion using an isotope ratio mass spectrometer (Finnigan Delta + XL) in an online continuous flow system. $\delta^{13}C_{leaf}$ was converted to Δ_{leaf} according to Farquhar et al. (1989), taking atmospheric $\delta^{13}C$ as 8.1‰, the average value recorded at the Cape Grim Air Pollution Station, Tasmania, in the 6 months prior to each sample collection campaign.

Deriving Photosynthetic Rate from Carbon Isotopic Composition

We estimated the maximum carboxylation capacity at 25°C (V_{cmax25} [μmol m^{-2} s^{-1}]) according to an empirical model that was derived from a meta-analysis of V_{cmax}, N_{area}, and LMA determined for 27 eucalypt species reported in 10 studies (Supplemental Table S4):

$$V_{cmax25} = 10^{1.7 - 0.5 \times \log N_{area} - 0.1 \times \log LMA - 0.4 \times \log N_{area} \times \log LMA} \quad (2)$$

V_{cmax25} was then converted to the actual velocity of Rubisco for carboxylation at ambient temperature (V_{cmax} [μmol m^{-2} s^{-1}]) according to Bernacchi et al. (2001) and the average daytime temperature of each site.

A time-integrated measure of leaf intercellular (and mesophyll) CO_2 mole fraction ($\bar{c}_i$ [μmol mol^{-1}]) was then estimated according to Farquhar et al. (1982):

$$\overline{c_i} = c_a\left(\frac{\Delta_{leaf} - 4.4}{22.6}\right) \quad (3)$$

where the atmospheric CO_2 mole fraction (c_a) was taken as 380 μmol mol^{-1}, reflecting the atmospheric partial pressure of CO_2 in 2003 (Keeling and Whorf, 2004). We assumed that photosynthesis was limited predominantly by carboxylation; therefore, the modeling constraints of Farquhar et al. (1982) and Sharkey et al. (2007) could be applied to yield an expression for time-integrated photosynthetic rate ($\bar{A}$ [μmol m^{-2} s^{-1}]):

$$\bar{A} = \left(1 - \frac{\Gamma*}{\overline{c_i}}\right)\frac{V_{cmax}\overline{c_i}}{\overline{c_i} + K_c(1 + O/K_O)} - R_d \quad (4)$$

Here, the mitochondrial respiration rate (R_d) was taken as 0.01 V_{cmax}, Γ* is the CO_2 compensation point in the absence of R_d, K_C and K_O are the Michaelis constants of Rubisco for carbon dioxide and oxygen, respectively, and O is the atmospheric partial pressure of oxygen. For values of these parameters and their temperature dependencies, we followed Bernacchi et al. (2001). We note that since $\bar{c}_i$ represents the mole fraction of CO_2 within both intercellular spaces and the mesophyll, the expression for $\bar{A}$ incorporates the drawdown in CO_2 at the sites of assimilation.

Statistical Analyses

Multiple relationships between traits were determined by PCA using OriginPro 2015. PCAs were conducted on both the larger data set comprising leaf morphological and hydraulic traits and the subset of data that included stomatal morphological traits. Data were log transformed to meet the assumption of normality, and z scores were calculated.

SMA regression analyses using R (version 3.0.2) and the SMATR package (Warton et al., 2006) were used to describe specific relationships between VLA, T_L, and d_x:d_y and the AI, based on the Atlas of Living Australia. Pairwise interactions between traits in the leaf morphological and stomatal morphological data sets were similarly quantified with SMA regression analyses. Data were log transformed prior to these analyses. These analyses were performed at the species-by-site level. We corrected for the potential effect of sampling bias due to relatedness between species in the relationships between VLA, T_L, and d_x:d_y and the AI by resampling the data at the taxonomic level of series (a subdivision of genus) using the taxonomic classification of Nicolle (2015). Our data set contains species from 11 distinct taxonomic series in this classification. Hence, each subsample contains 11 data points, with each data point being one species-site average and each species belonging to one of the 11 series. We used a bootstrap resampling strategy with replacement to obtain distributions of the taxonomically unbiased correlation r^2 and P value as well as the SMA from 10,000 random subsamples.

Linear regression models were developed to analyze the relationships between d_y and d_x, and to quantify the contribution of aridity, by including and excluding the site- and species-specific AI and the contribution of leaf morphology in terms of hypostomaty/amphistomaty in the models for the eucalypt sample. Linear regression models also were developed to analyze the relationship between the ratio d_x:d_y and the site- and species-specific AI. The traits d_x, d_y, and d_x:d_y as well as the AI were $\log_{10}$ transformed for the regression model analyses. The Matlab function fitlm was used to obtain the best least-squares fit of a model to the data.

We further tested our hypothesis on the coordination of aridity-induced changes in leaf morphological, hydraulic, and photosynthetic traits by analyzing the relative differences in several key traits between species that cooccur in the same site. Here, we first quantified the difference (Δ) in T_L, d_x:d_y, $\bar{A}$, and VLA relative to the difference in LMA (ΔLMA) between all different species that cooccur at each site:

$$\frac{\Delta Trait_X}{\Delta LMA}(i,j,n) = \frac{Trait_X(species_i, site_n) - Trait_X(species_j, site_n)}{LMA(species_i, site_n) - LMA(species_j, site_n)} \quad (5)$$

in which $Trait_X$ represents T_L, d_x:d_y, $\bar{A}$, and VLA, respectively, and the index i = 1 ... j-1 and the index j = 2 ... k, with k being the number of species that cooccur at each site, and the index n = 1 ... m, with m being the number of sites studied.

The observed differences in T_L, d_x:d_y, $\bar{A}$, and VLA relative to LMA were interpreted based on the sign of their average value. For example, if the average $\Delta T_L/\Delta LMA > 0$, it means that species with thicker leaves have, on average and within sites, higher LMA. We tested whether the means of these relative differences deviated from zero using a two-tailed Student's t test at a 5% significance level, including a Bonferroni correction considering four comparisons. We excluded comparisons of species with a difference in the denominator LMA of less than 2 μg cm^{-2}, which is equal to 5% of the total observed range in LMA.

Modeling Leaf Hydraulics and Photosynthesis

The potential advantage of reducing d_x:d_y below unity in terms of additional leaf gas exchange was quantified with a semiempirical model that relates l_{H2O} to k_{leaf} and subsequent transpiration and photosynthesis following Brodribb et al. (2007) and Brodribb and Feild (2010). Brodribb et al. (2007) provide an empirical expression for k_{leaf} that, given that atmospheric humidity and temperature are known, can be related to a transpiration flux and subsequent photosynthesis following Brodribb and Feild (2010). Principally, the model from Brodribb et al. (2007) relates leaf morphology and subsequent l_{H2O} (μm) to k_{leaf} (mmol MPa^{-1} m^{-2} s^{-1}) as:

$$k_{leaf} = 12,674 \cdot {l_{H_2O}}^{-1.26} \quad (6)$$

in which

$$l_{H_2O} = \tau\sqrt{dm_x{}^2 + d_y{}^2} \quad (7)$$

where τ is the curvature (or tortuosity) of the flow path through the leaf interior and assumed $\pi/2$, following Brodribb and Feild (2010), and dm_x is the intervein distances as defined by Brodribb and Feild (2010). We note that dm_x differs from the intervein distance d_x in our study. Brodribb et al. (2007) defined dm_x as the farthest equidistant point from surrounding veins. To apply our measurements of d_x to the model from Brodribb et al. (2007), we use the conversion $dm_x = 0.56 \times d_x$. This conversion was based on the difference in the relationships between dm_x and VLA as reported by Brodribb et al. (2007) and between d_x and VLA as obtained from our traced vein networks (Supplemental Fig. S2).

Brodribb and Feild (2010) use the expression for k_{leaf} to model the steady-state transpiration rate by assuming that the flow of (liquid) water into the leaf (E_l) equals the (gaseous) transpiration flux (E_g):

$$E_l = k_{leaf} \cdot \Delta\psi_{leaf} \quad (8)$$

$$E_g = g_{sw} \cdot (w_i - w_a) \quad (9)$$

where $\Delta\psi_{leaf}$ (MPa) is the water potential gradient across the leaf, g_{sw} (mol m^{-2} s^{-1}) is the stomatal conductance to water vapor, and $w_i - w_a$ (−) is the atmospheric humidity gradient between the leaf interior and the leaf exterior.

Brodribb and Feild (2010) approximated $\Delta\psi_{leaf}$ as constant (0.4 MPa) and based $w_i - w_a$ on the typical growth conditions of their species. With these assumptions, Equations 8 and 9 can be equated and rearranged to yield an expression for g_{sw} as a function of d_x and d_y.

For our analyses, we modified the geometrical relationships in the model framework from Brodribb and Feild (2010) and expressed k_{leaf} in terms of the traits d_x:d_y and T_L. Here, we invoked the assumption that $d_y = T_L/2$ (for empirical support, see Supplemental Data S1; Supplemental Fig. S1; Supplemental Table S2). For d_x, we inserted its relationship with the ratio d_x:d_y and the expression $d_y = T_L/2$, so that $d_x = \frac{d_x}{d_y}\frac{T_L}{2}$. Inserting both expressions in Equation 7 yields:

$$l_{H_2O} = \frac{1}{2\pi}\sqrt{\left(\frac{{T_L}^2}{4} + 0.078 \cdot \left(\frac{d_x}{d_y}\right)^2 \cdot {T_L}^2\right)} \quad (10)$$

Inserting this expression for l_{H2O} in Equation 6 yields, after rearranging, a semiempirical expression for k_{leaf} in terms of the leaf morphological traits d_x:d_y and T_L:

$$k_{leaf} = \frac{7140}{\left(\frac{{T_L}^2}{4} + 0.078 \cdot \left(\frac{d_x}{d_y}\right)^2 \cdot {T_L}^2\right)^{0.63}} \quad (11)$$

The expression above is subsequently used in an inverse approach to quantify the effect of changing d_x:d_y on photosynthesis as explained in the following.

We rearranged the Fick's law expression for stomatal diffusion of CO_2 to estimate the time-integrated stomatal conductance to CO_2 ($\overline{g_{sc}}$):

$$\overline{g_{sc}} = \overline{A} \cdot (c_a - \overline{c_i}) \quad (12)$$

Our measurements of $\delta^{13}C_{leaf}$ together with our approximation of V_{cmax25} provide information on $\overline{c_i}$ and $\bar{A}$ (Eqs. 3 and 4), which allow us to calculate $\overline{g_{sc}}$ for all our species-site combinations individually.

The time-integrated transpiration ($\bar{E}$) of each species-site combination was subsequently calculated as:

$$\bar{E} = 1.6 \cdot \overline{g_{sc}} \cdot (w_i - w_a) \quad (13)$$

For w_i, we assumed saturation at the annual average temperature for each site, and for w_a, we used the annual average humidity for each site, based on the climate data from the Atlas of Living Australia.

With $\bar{E}$ and k_{leaf} known, we subsequently approximated the time-integrated hydraulic pressure gradient across the leaf ($\Delta\overline{\Psi_{leaf}}$) for each species-site combination as:

$$\Delta\overline{\Psi_{leaf}} = \frac{\bar{E}}{k_{leaf}} \quad (14)$$

We then calculated the leaf hydraulic conductance of the theoretical optimal hydraulic architecture (k_{leaf_opt}) with d_x:$d_y = 1$, in combination with the observed T_L, using Equation 11. The transpiration of this theoretical optimal hydraulic architecture (E_{opt}) was then calculated assuming that $\Delta\overline{\Psi_{leaf}}$ remains unchanged from the value obtained using Equation 14:

$$E_{opt} = k_{leaf\_opt} \cdot \Delta\overline{\Psi_{leaf}} \quad (15)$$

The stomatal conductance to water vapor associated with this theoretical optimal leaf morphology (g_{sw_opt}) was calculated as:

$$g_{sw\_opt} = \frac{E_{opt}}{(w_i - w_a)} \quad (16)$$

The Rubisco-limited photosynthesis associated with the theoretical optimal leaf morphology ($\overline{A_{opt}}$) is modeled from Fick's law assuming that $g_{sc\_opt} = g_{sw\_opt}/1.6$:

$$\overline{A_{opt}} = g_{sc\_opt} \cdot \left(c_a - c_{i\_opt}\right) \quad (17)$$

In Equation 17, the leaf interior CO_2 concentration c_{i_opt} is unknown, but a second expression for steady-state photosynthesis as a function of c_i is obtained from the biochemical model of Farquhar et al. (1980) for Rubisco-limited photosynthesis while accounting for photorespiration (von Caemmerer, 2000) and mitochondrial respiration in light, as described in Equation 4. The two expressions for steady-state photosynthetic rate $\overline{A_{opt}}$ were iteratively solved for $c_i = c_{i\_opt}$ with a prescribed c_a of 380 μmol CO_2 mol^{-1} air, reflecting the atmospheric partial pressure of CO_2 in 2003 (Keeling and Whorf, 2004), using Matlab (version R2015b).

The above approach allows us to quantify the relative benefit of reducing d_x:d_y below unity on Rubisco-limited photosynthesis (δA [%]) for each species-site combination as:

$$\delta A = \frac{\bar{A} - \overline{A_{opt}}}{\bar{A}} \cdot 100 \quad (18)$$

We tested whether the average δA of our species-site combinations deviated from zero using a one-tailed Student's t test at a 5% significance level.

A sensitivity and uncertainty analysis of this model is provided in Supplemental Data S1 by exploring the effect of variability and uncertainty in model input parameters (Supplemental Table S5), on modeled photosynthesis (Supplemental Fig. S7), and δA (Supplemental Fig. S8).

Supplemental Data

The following supplemental materials are available.

Supplemental Figure S1. Relationship between vein depth and leaf thickness.

Supplemental Figure S2. Relationship between vein length per unit area and the intervein distance.

Supplemental Figure S3. Intervein distance to vein-epidermal distance ratio and site-specific AI of hypostomatous versus amphistomatous species.

Supplemental Figure S4. Effect of artificial aging on eucalypt leaf area and thickness.

Supplemental Figure S5. Statistics with correction for the classification based on Nicolle (2015).

Supplemental Figure S6. Paradermal image and cross section of a eucalypt leaf.

Supplemental Figure S7. Model sensitivity analysis.

Supplemental Figure S8. Model uncertainty analysis.

Supplemental Figure S9. Paradermal view of cleared and stained eucalypt leaves: *Corymbia aparrerinja*.

Supplemental Figure S10. Paradermal view of cleared and stained eucalypt leaves: *Eucalyptus gongylocarpa*.

Supplemental Figure S11. Paradermal view of cleared and stained eucalypt leaves: *Eucalyptus intertexta*.

Supplemental Figure S12. Paradermal view of cleared and stained eucalypt leaves: *Eucalyptus jacksonii*.

Supplemental Figure S13. Paradermal view of cleared and stained eucalypt leaves: *Eucalyptus marginata*.

Supplemental Figure S14. Paradermal view of cleared and stained eucalypt leaves: *Eucalyptus salmonophloia*.

Supplemental Figure S15. Paradermal view of cleared and stained eucalypt leaves: *Eucalyptus salmonophloia*.

Supplemental Figure S16. Paradermal view of cleared and stained eucalypt leaves: *Eucalyptus wandoo*.

Supplemental Table S1. Overview of the species, location, stomatal distribution, and climate variables.

Supplemental Table S2. SMA regression statistics for Supplemental Figure S1.

Supplemental Table S3. Regression models for the relationship between d_y and d_x.

Supplemental Table S4. Data used to model V_{cmax} from N_{area} and LMA.

Supplemental Table S5. Parameter ranges used in the model sensitivity and uncertainty analyses.

Supplemental Data S1. Species-by-site trait data.

ACKNOWLEDGMENTS

We thank Libby Trevenen and Hai Ngo (University of Western Australia) and Colin Crane (Department of Parks and Wildlife) for assistance with microscopy; Christiane Ludwig (Commonwealth Scientific and Industrial Research Organization-Agriculture) for laboratory assistance; Ines Hilker, Iris Kuhlmann, and Willi A. Brand (Max-Planck Institute for Biogeochemistry) for assistance with the leaf chemical analyses; and Grady Brand and Marty Brotherson for assistance with the collection of material from Kings Park.

Received August 23, 2016; accepted October 24, 2016; published October 26, 2016.

LITERATURE CITED

Bernacchi CJ, Singsaas EL, Pimentel C, Portis ARP Jr, Long SP (2001) Improved temperature response functions for models of Rubisco-limited photosynthesis. Plant Cell Environ **24:** 253–259

Blonder B, Buzzard V, Simova I, Sloat L, Boyle B, Lipson R, Aguilar-Beaucage B, Andrade A, Barber B, Barnes C, et al (2012) The leaf-area shrinkage effect can bias paleoclimate and ecology research. Am J Bot **99:** 1756–1763

Blonder B, Enquist BJ (2014) Inferring climate from angiosperm leaf venation networks. New Phytol **204:** 116–126

Blonder B, Violle C, Bentley LP, Enquist BJ (2011) Venation networks and the origin of the leaf economics spectrum. Ecol Lett **14:** 91–100

Bloom AJ, Chapin FS, Mooney HA (1985) Resource limitation in plants: an economic analogy. Annu Rev Ecol Syst **16:** 363–392

Boyce CK, Brodribb TJ, Feild TS, Zwieniecki MA (2009) Angiosperm leaf vein evolution was physiologically and environmentally transformative. Proc R Soc Lond B Biol Sci **276:** 1771–1776

Brodribb TJ, Feild TS (2010) Leaf hydraulic evolution led a surge in leaf photosynthetic capacity during early angiosperm diversification. Ecol Lett **13:** 175–183

Brodribb TJ, Feild TS, Jordan GJ (2007) Leaf maximum photosynthetic rate and venation are linked by hydraulics. Plant Physiol **144:** 1890–1898

Brodribb TJ, Feild TS, Sack L (2010) Viewing leaf structure and evolution from a hydraulic perspective. Funct Plant Biol **37:** 488–498

Brodribb TJ, Jordan GJ (2008) Internal coordination between hydraulics and stomatal control in leaves. Plant Cell Environ **31:** 1557–1564

Buckley TN, John GP, Scoffoni C, Sack L (2015) How does leaf anatomy influence water transport outside the xylem? Plant Physiol **168:** 1616–1635

Byrne M, Yeates DK, Joseph L, Kearney M, Bowler J, Williams MAJ, Cooper S, Donnellan SC, Keogh JS, Leys R, et al (2008) Birth of a biome: insights into the assembly and maintenance of the Australian arid zone biota. Mol Ecol **17:** 4398–4417

Chabot BF, Hicks DJ (1982) The ecology of leaf life spans. Annu Rev Ecol Syst **13:** 229–259

Choong MF, Lucas PW, Ong JSY, Pereira B, Tan HTW, Turner IM (1992) Leaf fracture-toughness and sclerophylly: their correlations and ecological implications. New Phytol **121:** 597–610

de Boer HJ, Eppinga MB, Wassen MJ, Dekker SC (2012) A critical transition in leaf evolution facilitated the Cretaceous angiosperm revolution. Nat Commun **3:** 1221

Drake PL, Froend RH, Franks PJ (2011) Linking hydraulic conductivity and photosynthesis to water-source partitioning in trees versus seedlings. Tree Physiol **31:** 763–773

Farquhar GD, Ehleringer JR, Hubick KT (1989) Carbon isotope discrimination and photosynthesis. Annu Rev Plant Physiol Plant Mol Biol **40:** 503–537

Farquhar GD, O'Leary MH, Berry JA (1982) On the relationship between carbon isotope discrimination and the intercellular carbon dioxide concentration in leaves. Aust J Plant Physiol **9:** 121–137

Farquhar GD, von Caemmerer S, Berry JA (1980) A biochemical model of photosynthetic CO_2 assimilation in leaves of C 3 species. Planta **149:** 78–90

Feild TS, Arens NC, Doyle JA, Dawson TE, Donoghue MJ (2004) Dark and disturbed: a new image of early angiosperm ecology. Paleobiology **30:** 82–107

Feild TS, Brodribb TJ, Iglesias A, Chatelet DS, Baresch A, Upchurch GR Jr, Gomez B, Mohr BAR, Coiffard C, Kvacek J, et al (2011) Fossil evidence for Cretaceous escalation in angiosperm leaf vein evolution. Proc Natl Acad Sci USA **108:** 8363–8366

Flexas J, Niinemets U, Gallé A, Barbour MM, Centritto M, Diaz-Espejo A, Douthe C, Galmés J, Ribas-Carbo M, Rodriguez PL, et al (2013) Diffusional conductances to CO_2 as a target for increasing photosynthesis and photosynthetic water-use efficiency. Photosynth Res **117:** 45–59

Franks PJ (2006) Higher rates of leaf gas exchange are associated with higher leaf hydrodynamic pressure gradients. Plant Cell Environ **29:** 584–592

Franks PJ, Drake PL, Beerling DJ (2009) Plasticity in maximum stomatal conductance constrained by negative correlation between stomatal size and density: an analysis using *Eucalyptus globulus*. Plant Cell Environ **32:** 1737–1748

Franks PJ, Farquhar GD (2001) The effect of exogenous abscisic acid on stomatal development, stomatal mechanics, and leaf gas exchange in *Tradescantia virginiana*. Plant Physiol **125:** 935–942

Gandolfo MA, Hermsen EJ, Zamaloa MC, Nixon KC, González CC, Wilf P, Cúneo NR, Johnson KR (2011) Oldest known *Eucalyptus* macrofossils are from South America. PLoS ONE **6:** e21084

Gillison AN (1981) Toward a functional vegetation classification. *In* AN Gillison, DJ Anderson, eds, Vegetation Classification in Australia. CSIRO and Australian National University Press, Canberra, Australia, pp 30–41

Givnish TJ, Pires JC, Graham SW, McPherson MA, Prince LM, Patterson TB, Rai HS, Roalson EH, Evans TM, Hahn WJ, et al (2005) Repeated evolution of net venation and fleshy fruits among monocots in shaded habitats confirms a priori predictions: evidence from an ndhF phylogeny. Proc Biol Sci **272:** 1481–1490

Grubb PJ (1998) A reassessment of the strategies of plants which cope with shortages of resources. Perspect Plant Ecol Evol Syst **1:** 3–31

Hopper SD (2003) An evolutionary perspective on south-west Western Australian landscapes, biodiversity and fire: a review and management implications. *In* IBN Abbott, ed, Fire in Ecosystems of South-West Western Australia: Impacts and Management. Backhuys Publishers, Leiden, The Netherlands, pp 9–35

Keeling CD, Whorf TP (2004) Atmospheric CO_2 concentrations derived from flask air samples at sites in the SIO network. *In* Trends: A Compendium of Data on Global Change. Carbon Dioxide Information Analysis Center, Oak Ridge National Laboratory, U.S. Department of Energy, Oak Ridge, TN

King DA (1997) The functional significance of leaf angle in *Eucalyptus*. Aust J Bot **45:** 619–639

Ladiges PY, Udovicic F, Nelson G (2003) Australian biogeographical connections and the phylogeny of large genera in the plant family Myrtaceae. J Biogeogr **30:** 989–998

Li L, McCormack ML, Ma C, Kong D, Zhang Q, Chen X, Zeng H, Niinemets Ü, Guo D (2015) Leaf economics and hydraulic traits are decoupled in five species-rich tropical-subtropical forests. Ecol Lett **18:** 899–906

Martin HA (2006) Cenozoic climatic change and the development of the arid vegetation in Australia. J Arid Environ **66:** 533–563

Middleton NJ, Thomas NSG (1997) World Atlas of Desertification. John Wiley & Sons, London

Mott KA, Gibson AC, Oleary JW (1982) The adaptive significance of amphistomatic leaves. Plant Cell Environ **5:** 455–460

Nicolle D (2015) Classification of the eucalypts (*Angophora*, *Corymbia* and *Eucalyptus*) version 2. http://www.dn.com.au/Classification-Of-The-Eucalypts.pdf

Niinemets U (2001) Global-scale climatic controls of leaf dry mass per area, density, and thickness in trees and shrubs. Ecology **82:** 453–469

Noblin X, Mahadevan L, Coomaraswamy IA, Weitz DA, Holbrook NM, Zwieniecki MA (2008) Optimal vein density in artificial and real leaves. Proc Natl Acad Sci USA **105:** 9140–9144

Poot P, Veneklaas EJ (2013) Species distribution and crown decline are associated with contrasting water relations in four common sympatric eucalypt species in southwestern Australia. Plant Soil **364:** 409–423

Price CA, Weitz JS (2014) Costs and benefits of reticulate leaf venation. BMC Plant Biol **14:** 234

Reich PB, Walters MB, Ellsworth DS (1992) Leaf life-span in relation to leaf, plant, and stand characteristics among diverse ecosystems. Ecol Monogr **62:** 365–392

Sack L, Dietrich EM, Streeter CM, Sánchez-Gómez D, Holbrook NM (2008) Leaf palmate venation and vascular redundancy confer tolerance of hydraulic disruption. Proc Natl Acad Sci USA **105:** 1567–1572

Sack L, Frole K (2006) Leaf structural diversity is related to hydraulic capacity in tropical rain forest trees. Ecology **87:** 483–491

Sack L, Holbrook NM (2006) Leaf hydraulics. Annu Rev Plant Biol **57:** 361–381

Sack L, Scoffoni C (2013) Leaf venation: structure, function, development, evolution, ecology and applications in the past, present and future. New Phytol **198:** 983–1000

Sack L, Scoffoni C, John GP, Poorter H, Mason CM, Mendez-Alonzo R, Donovan LA (2014) Leaf mass per area is independent of vein length per area: avoiding pitfalls when modelling phenotypic integration (reply to Blonder et al. 2014). J Exp Bot **65:** 5115–5123

Schulze ED, Turner NC, Nicolle D, Schumacher J (2006) Leaf and wood carbon isotope ratios, specific leaf areas and wood growth of Eucalyptus species across a rainfall gradient in Australia. Tree Physiol **26:** 479–492

Schymanski SJ, Or D, Zwieniecki M (2013) Stomatal control and leaf thermal and hydraulic capacitances under rapid environmental fluctuations. PLoS ONE **8:** e54231

Scoffoni C, Rawls M, McKown A, Cochard H, Sack L (2011) Decline of leaf hydraulic conductance with dehydration: relationship to leaf size and venation architecture. Plant Physiol **156:** 832–843

Sharkey TD, Bernacchi CJ, Farquhar GD, Singsaas EL (2007) Fitting photosynthetic carbon dioxide response curves for C3 leaves. Plant Cell Environ **30:** 1035–1040

Sommerville KE, Sack L, Ball MC (2012) Hydraulic conductance of *Acacia* phyllodes (foliage) is driven by primary nerve (vein) conductance and density. Plant Cell Environ **35:** 158–168

Steane DA, Nicolle D, McKinnon GE, Vaillancourt RE, Potts BM (2002) Higher-level relationships among the eucalypts are resolved by ITS-sequence data. Aust Syst Bot **15:** 49–62

Steane DA, Nicolle D, Sansaloni CP, Petroli CD, Carling J, Kilian A, Myburg AA, Grattapaglia D, Vaillancourt RE (2011) Population genetic analysis and phylogeny reconstruction in *Eucalyptus* (Myrtaceae) using high-throughput, genome-wide genotyping. Mol Phylogenet Evol **59:** 206–224

von Caemmerer S (2000) Biochemical Models of Leaf Photosynthesis, Vol 2. CSIRO Publishing, Collingwood, Australia

Warton DI, Wright IJ, Falster DS, Westoby M (2006) Bivariate line-fitting methods for allometry. Biol Rev Camb Philos Soc **81:** 259–291

Wright IJ, Reich PB, Cornelissen JHC, Falster DS, Groom PK, Hikosaka K, Lee W, Lusk CH, Niinemets U, Oleksyn J, et al (2005) Modulation of leaf economic traits and trait relationships by climate. Glob Ecol Biogeogr **14:** 411–421

Wright IJ, Reich PB, Westoby M, Ackerly DD, Baruch Z, Bongers F, Cavender-Bares J, Chapin T, Cornelissen JHC, Diemer M, et al (2004) The worldwide leaf economics spectrum. Nature **428:** 821–827

Wright IJ, Westoby M (2002) Leaves at low versus high rainfall: coordination of structure, lifespan and physiology. New Phytol **155:** 403–416

Zwieniecki MA, Boyce CK (2014) Evolution of a unique anatomical precision in angiosperm leaf venation lifts constraints on vascular plant ecology. Proc R Soc B Biol Sci **281:** 7